PCCP

Cite this: *Phys. Chem. Chem. Phys.*, 2012, **14**, 2078–2086

www.rsc.org/pccp

PAPER

Photophysics of indole-2-carboxylic acid in an aqueous environment studied by fluorescence spectroscopy in combination with *ab initio* calculations†

Annemarie Huijser,‡*[a] Michał F. Rode,[b] Alice Corani,[a] Andrzej L. Sobolewski[b] and Villy Sundström*[a]

Received 16th September 2011, Accepted 7th December 2011
DOI: 10.1039/c2cp22958g

The photo-physics and -chemistry of indoles are known to be highly complex and strongly dependent on their precise molecular structure and environment. Combination of spectroscopic analysis with quantum chemical calculations should be a powerful tool to unravel precise excited state deactivation mechanisms. At the same time, combined studies are seldom and likely far from trivial. In this work we explore the feasibility of combining spectroscopic and quantum-chemical data into one consistent model. The molecule of choice is indole-2-carboxylic acid (ICA) in aqueous media. Excited state dynamics are determined by time-resolved fluorescence experiments, while excited state reaction pathways of ICA–H_2O clusters are explored by *ab initio* calculations.

1. Introduction

Indoles form a broad class of molecules found throughout nature, with intriguing and very complex photophysical properties. Especially the amino acid tryptophan has been extensively studied and a matter of debate during several decades.[1–8] Suggested excited state reactions include proton transfer,[9,10] electron transfer,[9,11] intersystem crossing[5,12] and photoionization.[4,5,13] The photophysical properties are known to be particularly sensitive to environmental conditions such as the solvent,[13] temperature[2,5] and pH,[2,14] affecting the molecular geometry and solute–solvent interaction and in turn excited state reactions.

Another major source of natural indoles involves the eumelanin pigment present in the human skin. Eumelanin is a highly complex macromolecule based on indole derivatives 5,6-dihydroxyindole (DHI) and 5,6-dihydroxyindole-2-carboxylic acid (DHICA).[15,16] It is still a major question whether eumelanin protects the skin against UV-induced damage or becomes mutagenic upon UV-exposure. Spectroscopic analyses of the functionality and the underlying UV-induced reaction mechanisms of the full eumelanin pigment have appeared to be an almost impossible task. Responsible factors involve the highly complex pigment structure in combination with the largely unknown photophysical properties of the pigment building blocks.[17,18] This has especially recently been motivating researchers to perform quantum-chemical and spectroscopic studies on the small building blocks DHI and DHICA, with the aim to utilize the achieved insights to characterize model systems with increasing complexity and ultimately the full eumelanin pigment.[19–23]

Recent *ab initio* studies on DHI propose excited state deactivation to occur *via* intramolecular hydrogen atom transfer from the 5-hydroxyl group towards the adjacent 4-carbon atom (for enumeration, see Fig. 1).[21] Transient absorption measurements suggest excited state deactivation in DHI to occur through three parallel decay pathways involving (i) formation of a radical cation and solvated electron, (ii) intersystem crossing and (iii) radiative and non-radiative decay.[24] Very recent experiments performed by us demonstrate in addition a strong impact of the excitation energy, with formation of the radical cation and solvated electron more favorable at higher photon energies.[25]

Also the excited state deactivation mechanisms in DHICA have been a topic of interest in several recent studies. An important aspect to consider is that under physiologically relevant conditions the DHICA molecule could occur in two states: the neutral state and the mono-anion. Quantum-chemical studies on the DHICA mono-anion propose two ground state geometries: (i) a catechol anion with the 6-hydroxyl group deprotonated and (ii) the carboxylate anion. Both states are proposed to undergo an Excited State Intramolecular Proton Transfer (ESIPT) process upon excitation, leading to the same catechol

[a] *Department of Chemical Physics, Lund University, Box 124, 22100 Lund, Sweden. E-mail: Villy.Sundstrom@chemphys.lu.se; Fax: +46 46 22 24 119*
[b] *Institute of Physics, Polish Academy of Sciences, Al. Lotników 32/46, PL-02668 Warsaw, Poland*

† Electronic supplementary information (ESI) available. Discrete *vs.* continuum description of the water, effect of the water cluster size on the absorption and fluorescence spectrum, potential energy profiles relevant for photophysics of the isolated system, comparison of the cluster model (CM) with the single model (SM) system, computational methodology aspects concerning the correct description of the CM, *e.g.* the correct ordering of the excited states. See DOI: 10.1039/c2cp22958g

‡ Permanent address: Optical Sciences Group, Faculty of Science and Technology, MESA+ Institute for Nanotechnology, University of Twente, P.O. Box 217, 7500 AE Enschede, The Netherlands.

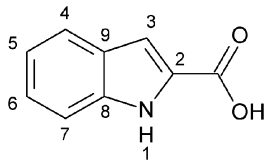

Fig. 1 Chemical structure of indole-2-carboxylic acid (ICA) with the enumeration of atoms indicated.

anion with the 5-hydroxyl group deprotonated.[20] Recent time-resolved fluorescence studies we performed however strongly suggest that in the ground state it is the carboxylate anion which is the dominating species and this state does not undergo major geometrical changes upon excitation. For neutral DHICA, the same study gives strong experimental evidence for the occurrence of sub-ps ESIPT between the protonated carboxylic acid group and the indole nitrogen, with the carboxylic acid group most likely acting as a proton donor.[26] Still to be addressed are the role of solvent molecules and the precise geometry of the zwitterionic state formed.

A very powerful tool to unravel and understand excited state reaction mechanisms and identify the precise geometry of photoproducts formed involves the combination of spectroscopic analysis with quantum-chemical calculations. Above-discussed works on DHI and DHICA however illustrate that combination of spectroscopic and computational studies into one consistent picture may be far from trivial. Indeed, combined experimental and theoretical works on indole derivatives are rather unusual. A likely reason for the discrepancy between experimental and computational data involves the solvent and its impact on optimal ground state geometries and excited state reactions. The aim of this work is to investigate the feasibility and usability of a combined spectroscopic and quantum-chemical study, with the latter taking into account solvent molecules. The molecule of choice is indole-2-carboxylic acid (ICA, chemical structure shown in Fig. 1), both in the anionic (ICA-A) and neutral states (ICA-N), as a first amenable step towards computational studies of the more complex DHICA and its higher oligomers. Excited state dynamics are determined by time-resolved fluorescence, while optimal ground state geometries and excited state reaction pathways are explored by *ab initio* calculations.

2. Experimental

Samples

Indole-2-carboxylic acid (ICA) and sodium phosphate buffers in H_2O (molarity of 0.1 M at pH 2.5, 0.02 M at pH 7.0) were purchased from Sigma-Aldrich.

Steady-state optical characterization

Absorption spectra were measured by using an Agilent spectrophotometer. Steady-state fluorescence spectra were recorded using a Spex Fluorolog spectrofluorometer and observed to be independent of excitation energy in the studied range of 4.2–5.0 eV.

Streak camera experiments

The streak camera setup used was described in detail earlier.[26] Briefly, UV-pulses with a central wavelength of 280 nm (4.43 eV), pulse energy of 3 pJ, duration of approximately 250 fs and a repetition rate of 8 MHz were focused on the sample using a 100 mm focal length quartz lens. The sample solution was kept under N_2 in a rotating cuvette with an optical path length of 2 mm. The concentration was determined from the optical density (OD, value of 0.20 at 280 nm) and literature values for the extinction coefficient[27] to be approximately 3×10^{-4} M. The fluorescence was collected at a magic angle and sent into a spectrograph (Chromex, 50 lines mm^{-1}, blazed at 600 nm) and streak camera setup (Hamamatsu, C6860). Experimental data were corrected for background and shading. Significant chemical degradation due to illumination was excluded on the basis of similar optical absorption spectra before and after the experiments. The fluorescence dynamics were observed to be neither dependent on the pulse energy (within the range of 1–10 pJ $pulse^{-1}$), nor on the optical density (in the range of 0.05–0.50 at 280 nm).

Single photon counting experiments

The single photon counting setup used was described in detail before.[26] Briefly, UV-pulses with a central wavelength of 280 nm, pulse energy of about 3 pJ, duration of about 1–2 ps and repetition rate of 4 MHz were used for excitation. The sample solution (OD at 280 nm = 0.18) was kept in a quartz cuvette with an optical path length of 10 mm. Similar optical absorption spectra before and after the experiments ruled out the occurrence of significant chemical degradation. The emitted photons were collected under magic angle conditions.

3. Computational methods

Methods in use

Ab initio calculations for all the model systems were performed with the TURBOMOLE program package,[28] making use of the Resolution-of-the-Identity (RI) approximation for the evaluation of the electron-repulsion integrals.[29] The equilibrium geometries of the molecular systems, both in the neutral and anionic states, in their closed-shell singlet ground state (S_0) were determined with the MP2 method.[30] Excitation energies, equilibrium geometries, and response properties of the lowest excited singlet states were calculated using the CC2 method[31,32] making use of the recently implemented CC2 analytic gradients.[33]

Molecular systems studied

Two types of systems were considered in the calculations. The first involves a single molecule (SM) in vacuum to explore the possible occurrence of any ESIPT reaction. The second system studied involves a cluster model (CM) consisting of the ICA molecule interacting with three water molecules. This number was observed to be an absolute minimum to imitate the first solvation sphere around the ICA molecule, saturating the hydrogen-bonding-to-the-solvent capacity of the system. Since the ICA molecule has three potential proton donating or accepting centers, the indole nitrogen and the two oxygen atoms of the carboxylic group, these atomic centers should all be involved in hydrogen bonding with water molecules. More details regarding this aspect are collected in the ESI.† Both SM and CM systems were studied in the neutral and the anionic form.

Basis sets used

For the SM system, both for the S_0 and S_1 electronic states, the Polarized Valence Double Zeta basis set (cc-pVDZ)[34] was used for geometry optimization. For the CM system, the basis set used in geometry optimization was augmented with diffuse functions to properly reproduce the geometries of intermolecular bonds in the cluster (aug-cc-pVDZ).[34] As shown by Xantheas *et al.*[35–37] this basis set accurately reproduces the geometries and the electric properties of the isolated molecules and their complexes. In the final calculations of adiabatic S_1 energies and vertical excitation energies, the Augmented Polarized Valence Triple Zeta basis set (aug-cc-pVTZ) was used in the case of SM at the S_0-geometries optimized with the cc-pVDZ basis set.

Minimum-energy pathways

The minimum energy profiles along the photophysically relevant reaction coordinates in the lowest singlet excited states were also determined using the CC2 method. Inspection of the optimized excited state geometries allowed identification of coordinates that can drive the relaxation process from the initially excited state to the ground state. After the choice of the relevant coordinate, the minimum energy path was calculated following this driving coordinate; all other nuclear degrees of freedom were optimized for a given value of this coordinate. For determination of S_1-state minima optimization was performed without any symmetry constraint, which leads to the local-minimum structure. On the other hand, the distinguished-coordinates approach used here allows for prediction of the transition-state-structures along the minimum energy pathways linking the local minimum structures. Such determined barriers are rough estimates of real saddle points in the case of strong curvature of the minimum-energy path, which is typical when the electronic nature ($\pi\pi^*$ *vs.* $n\pi^*$ in this case) of the excited state changes along the path.

4. Results and discussion

4.1. Ground state species and optical absorption properties

For the purpose of this study, the photophysical properties of ICA have been investigated in neutral and acidic sodium phosphate buffered H_2O. The pK_a of the carboxylic acid of ICA amounts to 3.69.[38] This implies that at pH 7.0 the quantity of deprotonated states (*i.e.* ICA-A) exceeds 99.9%. At pH 2.5 the situation is rather different with 94% of the molecules fully protonated (*i.e.* ICA-N) and 6% still deprotonated. Measurements at pH 2.5 have been performed at a buffer concentration of 0.1 M; the buffer concentration at pH 7.0 has however been kept as low as 0.02 to suppress complex formation between ICA-A and buffer constituents.[26] Fig. 2 shows the optical density (OD) spectra of the samples studied. ICA at pH 7.0, with ICA-A by far the dominating species, features a minor shoulder at around 4.1 eV, a strong band at 4.32 eV and higher absorption bands above 5 eV. The most noticeable impact on going from pH 7.0 to pH 2.5 involves a somewhat increased absorption strength and a bathochromic shift from 4.32 eV towards 4.25 eV. The red-most absorption band is for the anionic form composed of transitions from the ground state to three excited states (S_1, S_2, and S_3, see Table 1 or Table S1, ESI†) and for the neutral form transitions from the ground state to two excited states (S_1 and S_2, Table 1 or Table S1, ESI†). The calculated oscillator strengths for these transitions (Table 1 or Table S1, ESI†) suggest that the integrated absorbance of this band should be approximately 2.5 times stronger for the neutral molecule as compared to the anionic form. The spectra in Fig. 2 show that indeed the neutral form has stronger absorbance than the anionic form, but with a factor of $\sim$1.2. This discrepancy between calculation and experiment is understandable in view of the approximately factor of two precision of the calculated oscillator strengths. The observed red-shift of the $\sim$4.3 eV band on going from pH 7 to pH 2.5 is correctly predicted by the calculations as a result of the increased oscillator strength of the S_0–S_2 transition of the neutral state, while the anionic form has its oscillator strength distributed approximately evenly over the S_0–S_2 and S_0–S_3 transitions (see Table 1 and Table S1, ESI†).

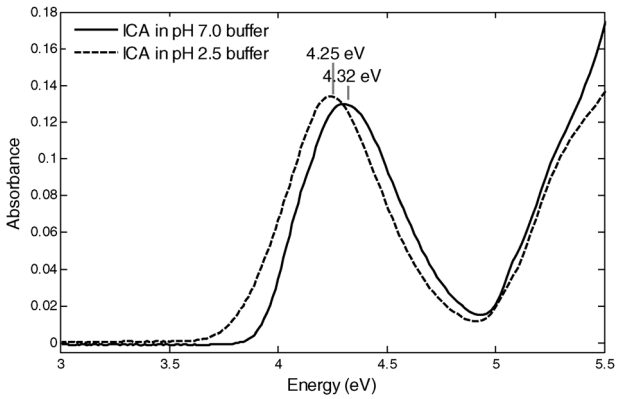

Fig. 2 Absorption spectra of ICA in 0.02 M pH 7.0 and 0.1 M pH 2.5 sodium phosphate buffers.

Table 1 Ground-state and vertical excitation energies (E), oscillator strengths (f) and dipole moments (μ) for the ground state minima of ICA-A (S_0(A-keto)) and ICA-N (S_0(N-*cis*) and S_0(N-*trans*)), calculated with the CC2/aug-cc-pVDZ method at the MP2/aug-cc-pVDZ ground-state equilibrium geometries. Experimental absorption values related to particular optical transitions are presented between brackets

S_0(A-keto)			S_0(N-*cis*)			S_0(N-*trans*)		
	E/eV	f	E/eV	f	μ/D	E/eV	f	μ/D
S_0	0.00		0.00		2.31	0.08		2.66
S_1	4.27 ($^1\pi\sigma^*$)	0.0013	4.17 ($^1\pi\pi^*$) [$\sim$4.0]	0.048	2.70	4.23 ($^1\pi\pi^*$) [$\sim$4.0]	0.048	2.59
S_2	4.39 ($^1\pi\pi^*$) [$\sim$4.1]	0.095	4.43 ($^1\pi\pi^*$) [4.25]	0.483	2.24	4.46 ($^1\pi\pi^*$) [4.25]	0.453	2.58
S_3	4.55 ($^1\pi\pi^*$) [4.32]	0.117	5.25	0.002	2.20	5.20	0.003	2.06

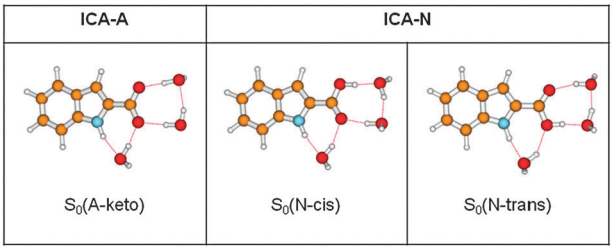

Fig. 3 Ground state equilibrium geometries of ICA-A: S_0(A-keto) and ICA-N: S_0(N-*cis*) and S_0(N-*trans*), optimized at the MP2/aug-cc-pVDZ level.

Before exploring computationally the excited state reaction pathways, it is clearly important to know which geometries are most favorable to occur in the ground state. The experimental conditions have been mimicked in the computational studies by surrounding the ICA molecule with three water molecules, as motivated in Section 3. Various ICA-A species are expected to coexist in the ground state. Their common features involve a protonated indole nitrogen and a deprotonated carboxylic acid group. They differ from each other in terms of positions of the surrounding three water molecules and the hydrogen bonding pattern. These geometries together form a branch of "A-keto"-like structures, of which the most stable one is shown in the left-hand panel of Fig. 3. Other A-keto structures are less stable with 0.1–0.2 eV. The calculated ground and excited state energies and transition oscillator strengths of the most stable form are presented in Table 1. The results with a larger aug-cc-pVTZ basis set, collected in the ESI†, Table S1, are close to the aug-cc-pVDZ results, indicating approaching the basis set limit. The S_0–S_1 transition is expected to be optically dark due to the dipole forbidden nature of the $\pi\sigma^*$ transition. Note that quantum chemical calculations using the CC2 method in general overestimate the energy involved in optical transitions with about 0.3 eV under the condition the basis set limit is reached.[39] Comparison of the experimental absorption spectrum shown in Fig. 2 with calculated values shows, thus, a good agreement and suggests that the shoulder at around 4.1 eV is related to S_0–S_2 excitation and the main absorption at 4.32 eV is due to S_0–S_3 excitation. The absorption above 5 eV is likely due to transitions to higher singlet states.

For the neutral molecule (ICA-N) the situation is different. Now two distinct, almost isoenergetic, stable ground states are expected to coexist; S_0(N-*cis*) and S_0(N-*trans*). Both possess protonated indole nitrogen and carboxylic acid functionalities, they however differ in terms of orientation of the carboxylic acid group (180° torsion around the single bond connecting the indole core with the carboxylic acid group) and hydrogen bonding pattern with the surrounding water molecules. The calculated ground and excited state energies and transition oscillator strengths of S_0(N-*cis*) and S_0(N-*trans*) are presented in Table 1. The S_0(N-*cis*) configuration is by 0.08 eV more stable as compared to the S_0(N-*trans*) form. Their optical absorption features are very similar. Comparison of the experimental absorption spectrum shown in Fig. 2 with calculated values presented in Table 1 shows good agreement (taking into account the computational overestimation of 0.3 eV[39]) and suggests that the tail in the spectrum at around 4.0 eV is due to S_0–S_1 excitation and the main absorption at 4.25 eV is related to S_0–S_2 excitation. The S_0–S_3 transition is expected to be optically dark, and the absorption above 5 eV is most likely due to transitions to levels beyond the S_3 state.

4.2. Fluorescence spectra and dynamics

Fig. 4 shows the fluorescence spectra of ICA in pH 7.0 (A) and pH 2.5 (B) buffers, including band analysis. Within an experimental range of 4.2 eV–5.0 eV, the fluorescence spectra do not depend on the excitation energy, demonstrating the absence of any relevant decay channel that might compete with internal conversion from higher states to the lowest excited state. Note that both spectra have a fluorescence band at 3.62 eV in common, although it is by far less intense at pH 2.5. Combining that with the fact that ICA-A is the dominating species at pH 7.0, but still present in significant amounts (6%) at pH 2.5, suggests that the band at 3.62 eV is due to ICA-A. The second minor band at pH 7.0 (at 3.10 eV) could be due to a complex formed between ICA-A and buffer constituents.[26] The main species at pH 2.5 involves ICA-N (94%). The band at 3.62 eV is already attributed to the 6% ICA-A present, the band at 3.04 eV can thus be ascribed to the 94% ICA-N. The only small difference in absorption spectra of these two species, the relative quantities, and weak emission leads to no observable excitation energy dependence of the fluorescence spectrum. Note that the band at 3.04 eV is only

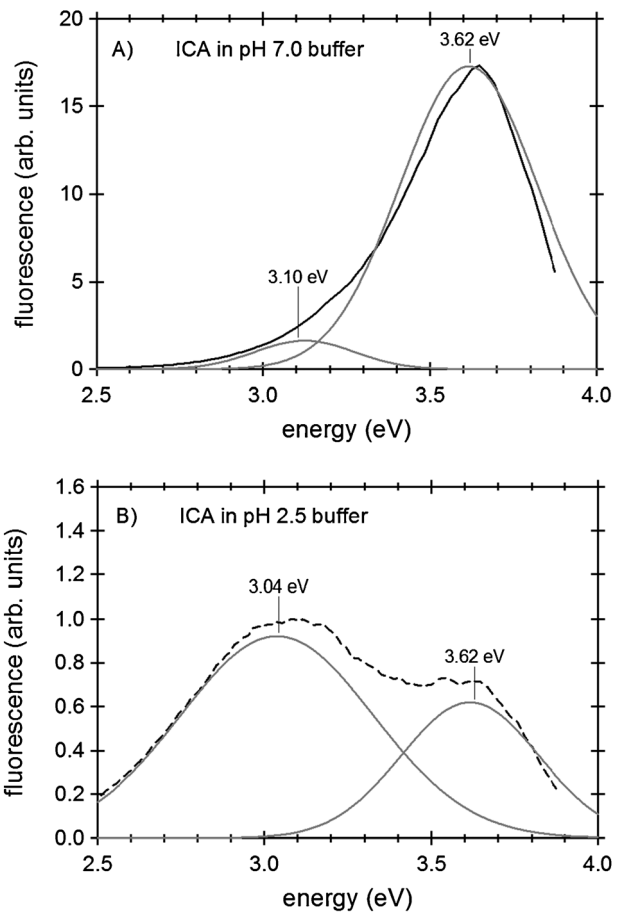

Fig. 4 Fluorescence spectra of ICA in 0.02 M pH 7.0 (A) and 0.1 M pH 2.5 (B) sodium phosphate buffers, including band analyses.

slightly more intense than the band at 3.62 eV, although the latter is only related to a minority ICA-A (6%) and the band at 3.04 eV is due to the 94% ICA-N. This suggests the presence of an important non-radiative decay channel for ICA-N.

Fig. 5 shows the fluorescence dynamics as a function of fluorescence energy of ICA in pH 7.0 (A) and pH 2.5 (B) buffers, recorded using streak camera detection. The dynamics of ICA in pH 7.0 buffer are fluorescence energy independent, which is in agreement with the observation of one major fluorescence band and a second only very minor band. The inset of Fig. 5A shows the decay at 3.6 eV recorded by single photon counting, covering a larger time window, including a fit by a mono-exponential decay function using a lifetime of 4.9 ns. This shows that excitation of ICA-A in the S_0(A-keto) geometry leads to an excited state emitting at 3.62 eV with an excited state lifetime of 4.9 ns. The fluorescence dynamics of ICA in pH 2.5 buffer (Fig. 5B) appear to depend on the fluorescence energy, which is in agreement with the dual fluorescence shown in Fig. 4B. The high-energy side dynamics are described by a bi-exponential decay function with lifetimes of 4.9 ns and 1.6 ns. The contribution of the 4.9 ns component is slightly lower than expected from the spectral analysis in Fig. 4B. This is likely due to the low sensitivity of the setup in the UV, leading to a high noise level, and the fact that the streak camera used is intended to measure short lifetimes (<2 ns) rather than longer lifetimes. The observation that the 4.9 ns lifetime observed at pH 2.5 equals that at pH 7.0 again confirms that both at pH 7.0 and pH 2.5 the fluorescence band at 3.62 eV is related to ICA-A. The low-energy side of the dynamics at pH 2.5 is accurately described by a mono-exponential decay function with a lifetime of 1.6 ns. Apparently, excitation of ICA-N, irrespective of whether in the S_0(N-*cis*) or S_0(N-*trans*) geometry, leads to an excited state that emits at 3.04 eV and has a lifetime of 1.6 ns. Combination of experimental data with *ab initio* calculations, discussed in the next section, will unravel whether the detected fluorescence is due to excited initial geometries or photoproducts. Also mechanisms for non-radiative decay will be presented.

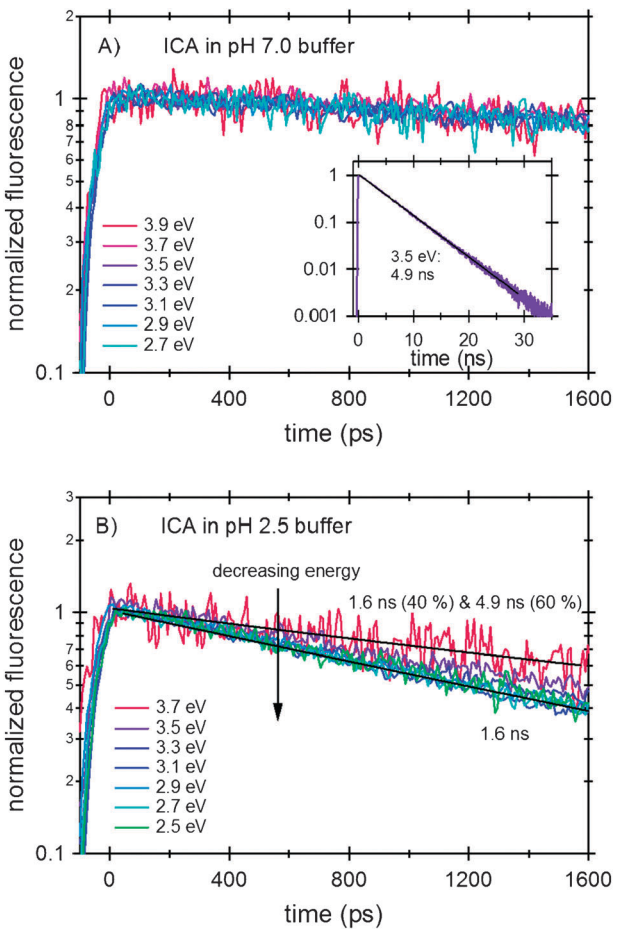

Fig. 5 Fluorescence dynamics of ICA in 0.02 M pH 7.0 (A) and 0.1 M pH 2.5 (B) sodium phosphate buffers as a function of fluorescence energy, including fits to mono- or bi-exponential decay functions and the resulting lifetimes.

4.3. Excited state processes

4.3.1. Anionic ICA (ICA-A). In contrast to the ground state, which has only one dominating minimum-energy geometry (S_0(A-keto)), the excited state energy landscape of ICA-A exhibits two distinct stable minima with the proton attached either to the nitrogen (the $^1\pi\pi^*$(A-keto) form) or to the oxygen atom (the $^1\pi\sigma^*$(A-enol) form). The difference in adiabatic energy between these two stable forms is 0.08 eV in favor of the latter. The S_1 minimum geometries along with the respective singly occupied HF orbitals describing the most important electronic configuration contributions of these two excited state minimum forms are shown in Fig. 6. The first geometry is formed directly upon optical excitation of the S_0(A-keto) form towards either the S_2 (shoulder in absorption spectrum) or S_3 excited state (strongest absorption), both of $\pi\pi^*$ character, and ultrafast internal conversion to the $^1\pi\pi^*$(A-keto) excited state minimum. Important to mention is the presence of a dark $^1\pi\sigma^*$ excited state, depicted as $S_1(^1\pi\sigma^*)$, lying just below $S_2(\pi\pi^*)$.The proximity of these two states gives the possibility of internal conversion from the $^1\pi\pi^*$ to the $^1\pi\sigma^*$ state followed by an ESIPT reaction resulting in the $^1\pi\sigma^*$(A-enol) form (right-hand panel of Fig. 6), which is 0.08 eV lower in adiabatic energy than the $^1\pi\pi^*$(A-keto) form. However, in order to form this state a barrier of 0.3 eV has to be passed, as

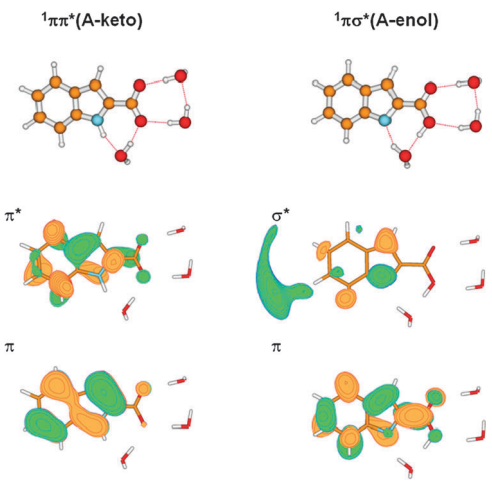

Fig. 6 Excited state equilibrium geometries of ICA-A: $^1\pi\pi^*$(A-keto) and $^1\pi\sigma^*$(A-enol), optimized at the CC2/aug-cc-pVDZ level and their respective singly occupied HF orbitals describing the most important electronic configuration contributions for a given state.

Table 2 Adiabatic energies (E) (relative to the ICA-A S_0(A-keto) minimum) and oscillator strengths (f) of the S_1–S_0 transition calculated at the excited state minimum of ICA-A, ground state energies calculated at the optimal geometry of the excited state minimum $S_0^{(S1)}$, and fluorescence energies for the given S_1-minimum calculated at the CC2/aug-cc-pVDZ level. Experimental fluorescence energies are presented between brackets

	$^1\pi\pi^*$(A-keto)		$^1\pi\sigma^*$(A-enol)	
	E/eV	f	E/eV	f
S_1	4.08	0.1258	4.00	0.0009
$S_0^{(S1)}$	0.30		0.67	
Fluorescence	3.78 [3.62]		3.33	

visualized in Fig. 8A. Assuming a pre-exponential factor in the order of 10^{13} s^{-1}, a typical value for a first order reaction,[40] and using the Arrhenius equation, this corresponds to a time scale in the order of 10 ns. In addition, the proton transfer process is possibly mediated by a single water molecule, which from the side of the indole nitrogen acts as a proton acceptor and at the same time it is a proton donor towards the carboxylate moiety. The calculated fluorescence properties of the $^1\pi\pi^*$(A-keto) and $^1\pi\sigma^*$(A-enol) forms are presented in Table 2. The $^1\pi\sigma^*$(A-enol) geometry is expected to be optically dark and therefore, in case it is formed, not detectable by fluorescence spectroscopy. The initial $^1\pi\pi^*$(A-keto) geometry, on the contrary, is expected to show a strong emission at 3.78 eV. This agrees well with the experimentally observed band at 3.62 eV considering that the CC2 method in general overestimates the energy involved in optical transitions with about 0.3 eV.[39,41] The observation that the $^1\pi\pi^*$(A-keto) has an excited state lifetime as long as 4.9 ns shows that the ESIPT process indeed occurs on a time scale of several nanoseconds or slower and is only a minor decay channel of the $^1\pi\pi^*$(A-keto) form. In case the formed $^1\pi\sigma^*$(A-enol) is not completely dark, but weakly emitting, it might to some extent contribute to the emission band at 3.10 eV attributed to complex formation between ICA-A and buffer constituents.

4.3.2. Neutral ICA (ICA-N). In the ground state, the neutral form of ICA (ICA-N) has two stable rotamers: S_0(N-*cis*) and S_0(N-*trans*), with the first being 0.08 eV more favorable. Optical excitation of these forms towards the weakly absorbing S_1 or strongly absorbing S_2 excited state followed by ultrafast internal conversion leads to the formation of the stable excited state minima $^1\pi\pi^*$(N-*cis*) and $^1\pi\pi^*$(N-*trans*), respectively. Except for these two minima, the excited state landscape however also shows a third stable minimum for a geometry depicted as $^1n\pi^*$(N-*trans*), see the right-hand panel of Fig. 7. This geometry differs significantly from the other two stable excited states, predominantly in terms of a large deformation of the carboxylic acid group. The hydroxyl group is tilted out from the indole molecular plane. Also the water molecules forming hydrogen bonds with the molecule are arranged in a non-planar fashion, forming a much more compact cluster. Note that also the dangling OH-proton is now positioned closer to the indole nitrogen as compared to both $^1\pi\pi^*$ geometries. The latter feature makes this $^1n\pi^*$(N-*trans*) excited state geometry a good candidate for being a preliminary intermediate for a further proton transfer reaction to take place from the carboxylic acid group towards the indole nitrogen. Proton transfer to the solvent

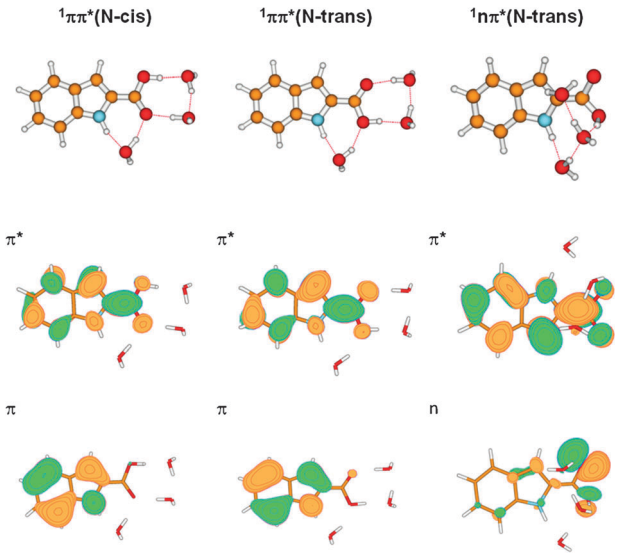

Fig. 7 Excited state equilibrium geometries of ICA-N: $^1\pi\pi^*$(N-*cis*), $^1\pi\pi^*$(N-*trans*) and $^1n\pi^*$(N-*trans*), optimized at the CC2/aug-cc-pVDZ level and their respective singly occupied HF orbitals describing the most important electronic configuration contributions.

(either the surrounding water molecules or the buffer constituents) can be excluded, since in that case similar fluorescence features would have been observed at pH 7.0 and pH 2.5.

The geometries along with their respective singly occupied HF orbitals describing the most important electronic configuration contributions of all three excited state minima are shown in Fig. 7. The calculated fluorescence properties of $^1\pi\pi^*$(N-*cis*), $^1\pi\pi^*$(N-*trans*) and $^1n\pi^*$(N-*trans*) are presented in Table 3. Apparently N-*cis* and N-*trans* are not only indistinguishable in terms of optical absorption, but also show very similar fluorescence features. This is due to a strong configurational mixing between nearly degenerated states. The calculated fluorescence energies of 3.51 eV and 3.63 eV agree reasonably well with the experimentally observed broad band at around 3.04 eV, although the theoretical overestimation exceeds the expected 0.3 eV. Possible reasons for this discrepancy have been explored by additional TD-DFT calculations for the CM system under vacuum and water, using the PCM model[42,43] in conjunction with the B3[44]-LYP[45,46] functional and the aug-cc-pVDZ basis set. These PCM/TD-DFT calculations were performed with the Gaussian 09 program package.[47] Calculated fluorescence energies for (i) a single ICA molecule (using CC2 method), (ii) an ICA–$(H_2O)_3$ cluster (using the CC2 and TD-DFT methods), and (iii) an ICA–$(H_2O)_3$ cluster (using the TDDFT method in conjunction with the PC model) are collected in Table S2 of the ESI.† These results show a step-wise decrease of the calculated fluorescence energy, with the highest value for a SM system under vacuum, smaller values for a CM system under vacuum, and a further decrease of the fluorescence energy value when the CM system was treated by the PCM model, suggesting that the overestimated fluorescence energy is a solvent effect.

The shorter lifetime of 1.6 ns of ICA-N as compared to the value of 4.9 ns for ICA-A is in disagreement with the two times smaller fluorescence oscillator strength of ICA-N, if excited state deactivation would occur entirely by radiative decay

Table 3 Adiabatic energies (E) (relative to the ICA-N S_0(N-*cis*) minimum) and oscillator strengths (f) of the S_1–S_0 transition calculated at the excited state minimum, ground state energies calculated at the optimal geometry of the excited state minimum $S_0^{(S1)}$, and fluorescence energies for the given S_1-minimum calculated at the CC2/aug-cc-pVDZ level. Experimental fluorescence energies are presented between brackets

	$^1\pi\pi^*$(N-*cis*)			$^1\pi\pi^*$(N-*trans*)			$^1n\pi^*$(N-*trans*)		
	E/eV	f	μ/D	E/eV	f	μ/D	E/eV	f	μ/D
S_1	3.82	0.060	5.0	4.04	0.058	4.7	3.99	0.0001	4.0
$S_0^{(S1)}$	0.31		1.5	0.41		2.0	2.13		3.7
Fluorescence	3.51 [3.04]			3.63 [3.04]			1.86		

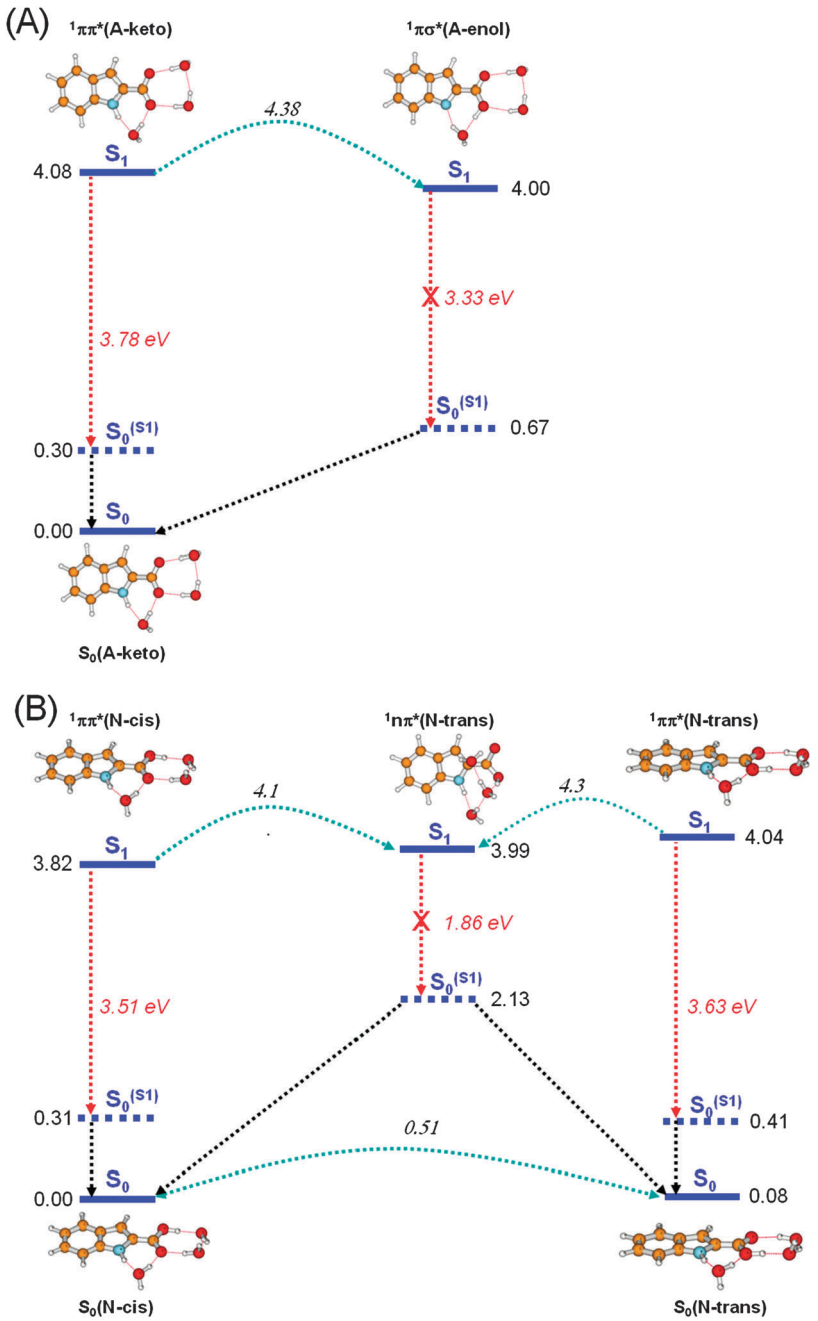

Fig. 8 Non-radiative excited state decay mechanism for the anionic $^1\pi\pi^*$ (A-keto) geometry (A) and for the neutral $^1\pi\pi^*$(N-*cis*) and $^1\pi\pi^*$(N-*trans*) geometries (B). Energy levels are in eV. The numbers at the dashed lines indicate the height of barriers relative to ground state energies.

(or the same degree of radiationless decay as ICA-A in addition to the radiative decay). Obviously, the excited state lifetime of ICA-N is to a large extent determined by non-radiative decay occurring on a nanosecond time scale, competing with fluorescence and decreasing the excited state lifetime and fluorescence quantum yield. Decay of initially formed excited states minima

$^1\pi\pi^*$(N-*cis*) and $^1\pi\pi^*$(N-*trans*) into $^1n\pi^*$(N-*trans*) as shown in Fig. 8B is a plausible explanation, although a barrier of 0.3 eV has to be passed, corresponding to a time constant in the order of nanoseconds, assuming an Arrhenius rate law decay with a pre-exponential factor of approximately 10^{13} s^{-1}.[40] The $^1n\pi^*$(N-*trans*) state formed is expected to be optically dark, providing as such an important non-radiative decay channel for the neutral system.

5. Conclusions

Combining spectroscopic and quantum-chemical data into one consistent model is a realistic and powerful approach, provided solute–solvent interactions are taken into account. In the case of ICA it appears to be sufficient to simulate the experimental aqueous environment by three water molecules saturating the hydrogen bonding capacity of the molecule. In the case of larger indole oligomers, likely more water molecules will be needed to achieve this effect. The photophysics and -chemistry of ICA strongly depend on the protonation stage. Anionic ICA (ICA-A) exhibits only one ground state equilibrium geometry, with the indole nitrogen protonated and the carboxylic acid deprotonated. This state is still stable upon optical excitation, although it could, except for decay to its ground state, also undergo a minor nanosecond ESIPT process from the indole nitrogen towards the deprotonated carboxylic acid group. The situation for neutral ICA (ICA-N) is more complicated in the sense that this state has two stable ground state geometries, with a 180° different torsion angle of the carboxylic acid group with respect to the indole molecular plane. Both geometries have comparable optical properties and are still stable after optical excitation. In the excited state they can however, except for decay to their corresponding ground state, also undergo deformation of the carboxylic group which can be considered as the preliminary step to partial or full ESIPT from the carboxylic acid group proton towards the indole nitrogen, providing an efficient mechanism of a non-radiative decay of the optically excited system.

Acknowledgements

Research performed in Lund was supported by funding from the Wenner-Gren Foundation, the Swedish Energy Agency, the Knut and Wallenberg Foundation and the Swedish Research Council funded Linnaeus program within the Lund Laser Centre. Jonas K. Hannestad, Department of Physical Chemistry of Chalmers University of Technology in Göteborg (Sweden) is acknowledged for performing the single photon counting measurement. Research performed in Warsaw was supported by the computational Grant G29-11 from the Interdisciplinary Centre for Mathematical and Computational Modeling. V.S. acknowledges the European Research Council for an Advanced Investigator Grant, 226136-VISCHEM.

References

1 R. W. Ricci, *Photochem. Photobiol.*, 1970, **12**, 67.
2 R. J. Robbins, G. R. Fleming, G. S. Beddard, G. W. Robinson, P. J. Thistletwaite and G. J. Woolfe, *J. Am. Chem. Soc.*, 1980, **102**, 6271.
3 J. W. Petrich, M. C. Chang, D. B. McDonald and G. R. Fleming, *J. Am. Chem. Soc.*, 1983, **105**, 3824.
4 W. G. McGimpsey and Gorner, *Photochem. Photobiol.*, 1996, **64**, 501.
5 K. L. Stevenson, G. A. Papadantonakis and P. R. LeBreton, *J. Photochem. Photobiol., A*, 2000, **133**, 159.
6 D. Nolting, C. Marian and R. Weinkauf, *Phys. Chem. Chem. Phys.*, 2004, **6**, 2633.
7 Z. J. Huang and Z. J. Lin, *J. Phys. Chem. A*, 2005, **109**, 2656.
8 D. Sharma, J. Leonard and S. Haacke, *Chem. Phys. Lett.*, 2010, **489**, 99.
9 A. G. Szabo and D. M. Rayner, *J. Am. Chem. Soc.*, 1980, **102**, 554.
10 E. Vöhringer-Martinez and A. Toro-Labbé, *J. Comput. Chem.*, 2010, **31**, 2642.
11 V. P. Kazakov, S. S. Ostakhov and G. G. Farrakhova, *High Energy Chem.*, 2008, **42**, 283.
12 D. V. Bent and E. Hayon, *J. Am. Chem. Soc.*, 1975, **114**, 2612.
13 P. S. Sherin, O. A. Snytnikova, Y. P. Tsentalovich and R. Z. Sagdeev, *J. Chem. Phys.*, 2006, **125**, 144511.
14 M. R. Eftink, Y. Jia, D. Hu and C. A. Ghiron, *J. Phys. Chem.*, 1995, **99**, 5713.
15 P. Meredith and T. Sarna, *Pigment Cell Res.*, 2006, **19**, 572.
16 M. d'Ischia, A. Napolitano, A. Pezzella, P. Meredith and T. Sarna, *Angew. Chem., Int. Ed.*, 2009, **48**, 3914.
17 J. B. Nofsinger and J. D. Simon, *Photochem. Photobiol.*, 2001, **74**, 31.
18 M. L. Tran, B. J. Powell and P. Meredith, *Biophys. J.*, 2006, **90**, 743.
19 P. Nighswander-Rempel Stephen, S. Olsen, B. Mahadevan Indumathy, G. Netchev, B. C. Wilson, S. C. Smith, H. Rubinsztein-Dunlop and P. Meredith, *Photochem. Photobiol.*, 2008, **84**, 613.
20 S. Olsen, J. Riesz, I. Mahadevan, A. Coutts, J. P. Bothma, B. J. Powell, R. H. McKenzie, S. C. Smith and P. Meredith, *J. Am. Chem. Soc.*, 2007, **129**, 6672.
21 A. L. Sobolewski and W. Domcke, *ChemPhysChem*, 2007, **8**, 756.
22 K. B. Stark, J. M. Gallas, G. W. Zajac, M. Eisner and J. T. Golab, *J. Phys. Chem. B*, 2003, **107**, 3061.
23 B. J. Powell, T. Baruah, N. Bernstein, K. Brake, H. McKenzie Ross, P. Meredith and M. R. Pederson, *J. Chem. Phys.*, 2004, **120**, 8608.
24 M. Gauden, A. Pezzella, L. Panzella, A. Napolitano, M. d'Ischia and V. Sundström, *J. Phys. Chem. B*, 2009, **113**, 12575.
25 A. Huijser, A. Pezzella and V. Sundstrom, *Phys. Chem. Chem. Phys.*, 2011, **13**, 9119.
26 A. Huijser, A. Pezzella, J. K. Hannestad, L. Panzella, A. Napolitano, M. d'Ischia and V. Sundstrom, *ChemPhysChem*, 2010, **11**, 2424.
27 P. R. Bangal and S. Chakravorti, *J. Phys. Chem. A*, 1999, **103**, 8585.
28 R. Ahlrichs, M. Bar, M. Haser, H. Horn and C. Kolmel, *Chem. Phys. Lett.*, 1989, **162**, 165.
29 F. Weigend and M. Haser, *Theor. Chem. Acc.*, 1997, **97**, 331.
30 C. Moller and M. S. Plesset, *Phys. Rev.*, 1934, **46**, 0618.
31 O. Christiansen, H. Koch and P. Jorgensen, *Chem. Phys. Lett.*, 1995, **243**, 409.
32 C. Hattig and F. Weigend, *J. Chem. Phys.*, 2000, **113**, 5154.
33 A. Kohn and C. Hattig, *J. Chem. Phys.*, 2003, **119**, 5021.
34 T. H. Dunning, *J. Chem. Phys.*, 1989, **90**, 1007.
35 S. S. Xantheas and T. H. Dunning, *J. Chem. Phys.*, 1993, **99**, 8774.
36 S. S. Xantheas, *J. Chem. Phys.*, 1994, **100**, 7523.
37 S. S. Xantheas and L. X. Dang, *J. Phys. Chem.*, 1996, **100**, 3989.
38 M. Rele, S. Kapoor, S. Hedge, S. Naumov and T. Mukherjee, *Res. Chem. Intermed.*, 2006, **32**, 637.
39 C. Hattig and K. Hald, *Phys. Chem. Chem. Phys.*, 2002, **4**, 2111.
40 R. A. Alberty and R. J. Silbey, *Physical Chemistry*, John Wiley & Sons, New York, 1992.
41 M. F. Rode and A. L. Sobolewski, *Chem. Phys.*, 2008, **347**, 413.
42 S. Miertus, E. Scrocco and J. Tomasi, *Chem. Phys.*, 1981, **55**, 117.
43 R. Cammi, S. Corni, B. Mennucci and J. Tomasi, *J. Chem. Phys.*, 2005, **122**, 104513.
44 A. D. Becke, *J. Chem. Phys.*, 1993, **98**, 5648.
45 C. Lee, W. Yang and R. G. Parr, *Phys. Rev. B: Condens. Matter*, 1988, **37**, 785.
46 B. Miehlich, A. Savin, H. Stoll and H. Preuss, *Chem. Phys. Lett.*, 1989, **157**, 200.

47 M. J. Frisch, G. W. Trucks, H. B. Schlegel, G. E. Scuseria, M. A. Robb, J. R. Cheeseman, G. Scalmani, V. Barone, B. Mennucci, G. A. Petersson, H. Nakatsuji, M. Caricato, X. Li, H. P. Hratchian, A. F. Izmaylov, J. Bloino, G. Zheng, J. L. Sonnenberg, M. Hada, M. Ehara, K. Toyota, R. Fukuda, J. Hasegawa, M. Ishida, T. Nakajima, Y. Honda, O. Kitao, H. Nakai, T. Vreven, J. A. Montgomery, Jr., J. E. Peralta, F. Ogliaro, M. Bearpark, J. J. Heyd, E. Brothers, K. N. Kudin, V. N. Staroverov, T. Keith, R. Kobayashi, J. Normand, K. Raghavachari, A. Rendell, J. C. Burant, S. S. Iyengar, J. Tomasi, M. Cossi, N. Rega, J. M. Millam, M. Klene, J. E. Knox, J. B. Cross, V. Bakken, C. Adamo, J. Jaramillo, R. Gomperts, R. E. Stratmann, O. Yazyev, A. J. Austin, R. Cammi, C. Pomelli, J. W. Ochterski, R. L. Martin, K. Morokuma, V. G. Zakrzewski, G. A. Voth, P. Salvador, J. J. Dannenberg, S. Dapprich, A. D. Daniels, O. Farkas, J. B. Foresman, J. V. Ortiz, J. Cioslowski and D. J. Fox, *Gaussian 09, Revision B.01*, Gaussian, Inc., Wallingford CT, 2010.

